Crystallization of Deformable Spherical Colloids

Vera M. O. Batista and Mark A. Miller

University Chemical Laboratories, Lensfield Road, Cambridge CB2 1EW, United Kingdom

(Received 16 April 2010; published 18 August 2010)

We introduce and characterize a first-order model for a generic class of colloidal particles that have a preferred spherical shape but can undergo deformations while always maintaining hard-body interactions. The model consists of hard spheres that can continuously change shape at fixed volume into prolate or oblate ellipsoids of revolution, subject to an energetic penalty. The severity of this penalty is specified by a single parameter that determines the flexibility of the particles. The deformable hard spheres crystallize at higher packing fractions than rigid hard spheres, have a narrower solid-fluid coexistence region and can reach high densities by a second transition to an orientationally ordered crystal.

DOI: 10.1103/PhysRevLett.105.088305 PACS numbers: 82.70.Dd, 64.70.D−, 82.70.Kj, 87.15.nt

The interactions between colloidal particles can often be described to a good approximation by simple potentials, making many colloids amenable to investigation through analytic theory and computer simulation as well as by experiment. An even greater advantage of a simple description is that it reveals the underlying similarities between apparently disparate systems. For example, hard spheres with square-well attraction provide a useful approximate account of spherical colloids with polymer-induced depletion attraction [1] as well as of suspensions of globular proteins [2], where the origin of the attraction is quite different.

Despite the success of hard spheres and square wells as generic representations of spherical colloids, these models must be refined to capture more specific properties of particular systems. One development of this kind currently receiving concentrated attention is anisotropic attraction. Such ''patchy'' interactions better capture the inhomogeneous surface of globular proteins [3] but can also be used to design particles that self-assemble into well-defined superstructures [4] or to control the dynamic properties of colloidal gels [5].

Here we address a different point that has received less attention so far, but which is also relevant to several types of colloid including globular proteins, micelles and emulsions. These systems have in common a hard repulsive core; i.e., the particles are effectively impenetrable on a scale comparable to their own diameter. However, this core is not strictly rigid. At any instant, a particle may deviate from an average spherical shape while remaining impenetrable to other particles. This internal flexibility will affect the microscopic structure, phase behavior and kinetics of the system, including any structural arrest. For example, the flexibility of proteins in solution is constrained in the crystal environment [6], suggesting that there may be an entropic contribution to the difficulty of crystallizing proteins in addition to energetic frustration at the crystal contacts [7]. The nonrigidity of individual protein molecules also contributes to the extreme softness of their crystals [7]. In the field of soft matter, the deformability of microgel spheres has recently been implicated in their ability to pass through pores much narrower than their spherical diameter [8] and plays a key role in controlling the fragility of glasses composed of such particles [9]. The droplets in surfactant-stabilized emulsions and in nonequilibrium nanoemulsions [10] are also impenetrable, yet nonrigid. Here, we introduce a general model for flexible hard colloids and characterize its equilibrium phase behavior, knowledge of which is essential for all subsequent investigations.

In the spirit of other archetypal models for colloids, our deformable hard spheres incorporate flexibility at the simplest possible level so that the effects of particle deformability can be isolated from other properties. At mechanical equilibrium, an isolated particle is taken to be a hard sphere of diameter σ. This sphere may deform into a prolate or oblate ellipsoid of revolution while preserving its volume at $\pi\sigma^3/6$. The distortion is quantified by the aspect ratio $x = a/b$ of the particle, which is the single new degree of freedom introduced for each particle. Here, a is the symmetry semiaxis length of the ellipsoid and b is the orthogonal semiaxis length. The constraint of fixed particle volume is appropriate for incompressible particles and means that a system with a fixed number of particles also has a fixed packing fraction. Although some colloids are both deformable and compressible, the purpose of the present model is to isolate and assess the specific effects of deformability. Naturally, more complex deformations are possible in many real systems, but elongation-flattening modes are often the first to become important [11]. In this sense, our model is a first-order approximation.

The extent to which a particle deviates from being spherical is controlled by an energetic penalty for the deformation. There are several possible choices for the energy function, depending on the application, but we have chosen a representative form with a liquid droplet in mind. For a droplet of fixed volume, the work required to deform it from a sphere is proportional to the surface tension γ and the increase ΔA in surface area. ΔA is a

computationally cumbersome and highly skewed function of x but, as shown in Fig. 1, it is a more symmetrical function of $\ln x$. We therefore expand the area about $\ln x = 0$ in a Taylor series to the quadratic term, giving the energy

$$U = \kappa(\ln x)^2, \tag{1}$$

like an internal spring restoring the particle to $x = 1$. Here, κ is the stiffness parameter, which in the case of the liquid droplet is related to the surface tension by $\kappa = 8\pi\sigma^2\gamma/45$. As well as its physical interpretation, a harmonic potential in $\ln x$ is appealing because it treats oblate and prolate ellipsoids with reciprocal aspect ratios as energetically equal. We note that there is a remarkable near symmetry between the prolate and oblate sides of the phase diagram of rigid hard ellipsoids [12]. If the energy is written in terms of the linear deformation $\delta = \sigma - a = \sigma(1 - x^{2/3})$, then U is quadratic in δ to leading order, so for small deformations our model is more akin to the spring model of liquid droplets than to the Hertz model for elastic spheres (representing, e.g., spheres of highly cross-linked polymers), where $U \propto \delta^{5/2}$ [13].

We now calculate the phase diagram of the deformable hard spheres to see how flexibility affects the thermodynamics of crystallization. In the limit $\kappa \to \infty$ of strong rigidity, the model reduces to hard spheres, which undergo a purely entropic phase transition between fluid and face-centered cubic (fcc) crystal phases with coexistence packing fractions of 0.492 and 0.543, respectively [14]. The packing fraction is defined by $\phi = (N\sigma^3/V)(\pi/6)$, where N is the number of particles in the volume V. For finite κ, the shape of each particle undergoes thermal fluctuations to an extent controlled by $\beta\kappa$, where β^{-1} is the thermal energy. To trace the fluid-crystal coexistence boundaries as a function of $\beta\kappa$ we need to find the packing fractions at which the pressures of the two phases are equal at the same time as their chemical potentials are equal.

Our Monte Carlo (MC) simulations employ separate translational, rotational, and deformation steps for individual particles, with uniformly distributed random Cartesian displacements, Euler angle rotations and changes to $\ln x$, respectively. Displacements and rotations are accepted unless an overlap is generated between ellipsoids, detected using the Perram-Wertheim algorithm [15], in which case they are rejected. A trial deformation from $\ln x$ to $\ln x'$ is also rejected if it generates an overlap but otherwise is accepted according to the Metropolis criterion.

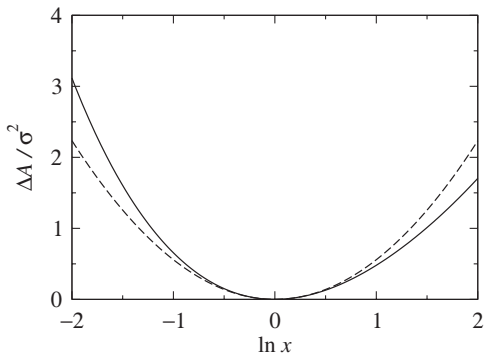

FIG. 1. Solid line: increase ΔA in surface area of an ellipsoid of revolution relative to a sphere of the same volume as a function of the logarithm of its aspect ratio x. Dashed line: quadratic expansion of ΔA in $\ln x$.

The equation of state was obtained for each phase using isothermal-isobaric simulations in which the pressure was imposed by isotropic changes to the length of the cubic, periodic simulation cell. Sufficiently system-size independent densities as a function of pressure were obtained with as few as $N = 108$ particles in some regions of the phase diagram, but N was increased to 432 where necessary. The length of simulations was similarly dependent on the conditions, with up to 2×10^7 MC sweeps for equilibrium sampling at the highest fluid densities.

The chemical potential of the fcc solid was obtained using the Frenkel-Ladd method [16,17], in which a thermodynamic integration is performed between the crystal and a reference Einstein crystal, where particles are tethered to the lattice sites and interactions are all but eliminated. At the same time as switching on the harmonic tethering potentials, a constraint was gradually applied to the deformation coordinates (effectively increasing κ) to force them to be nearly spherical, thereby suppressing interactions in the reference crystal due to the elongation of particles towards their neighbors. Since, even at the end of this process, the particles are not perfectly spherical, the small residual probability p_{nn} of overlap between tethered nearest neighbors must be evaluated by simulation to obtain its contribution

$$\Delta F_{\mathrm{nn}} = -N(n/2)\beta^{-1}\ln(1 - p_{\mathrm{nn}})$$

to the free energy [16]. Here, $n = 6$ is the number of nearest-neighbor pairs per particle. These free energy calculations employed constant-volume isothermal simulations of $N = 1372$ particles. For the fluid phase, the chemical potential was obtained by thermodynamic integration of the equation of state from a dilute gas. At low density, the additional work for stiffening the deformation coordinates to match the value reached in the Einstein crystal can be calculated analytically.

Using the equations of state and chemical potentials of the two phases calculated in this way, the coexisting densities were obtained at a series of values of $\beta\kappa$ as depicted by pairs of symbols in the phase diagram in Fig. 2. The intervals between the points were joined using Gibbs-Duhem integration [18].

As can be seen in Fig. 2, both the fluid and the crystal boundaries move monotonically to higher packing fractions with increasing particle flexibility. The fluid density is more strongly affected, resulting in a gradual narrowing of the coexistence region. These trends qualitatively resemble the effect of size polydispersity in hard spheres, where the compression required to crystallize a fluid in-

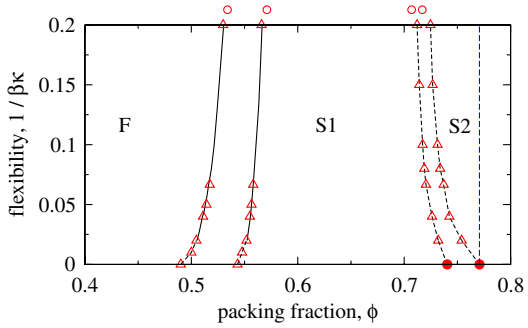

FIG. 2 (color online). Phase diagram of deformable hard spheres: fluid (F), fcc crystal of near-spheres (S1), crystal of ellipsoids (S2). Open triangles: coexistence points from free energy calculations. Solid circles: hypothetical infinite-pressure limit for the S1-S2 transition. Open circles: $\kappa = 0$ limit. Solid lines are from Gibbs-Duhem integration, while dashed lines are a guide to the eye. Vertical long-dashed line: maximum packing fraction of ellipsoids.

creases with the width of the particle-size distribution [19]. The deformable spheres, however, constitute a strictly a one-component system, despite the instantaneously differing shapes of the particles. Flexibility has delayed the transition from fluid to solid until higher density; i.e., at a given density, crystallization is inhibited. Snapshots of the fluid and crystal are shown in Figs. 3(a)–3(c).

Spherical particles can be packed to the same maximum of $\phi = \pi/\sqrt{18} = 0.7405\ldots$ by stacking hexagonal layers in an fcc ($ABCABC\ldots$), hexagonally close-packed (hcp, $ABAB\ldots$) or random sequence. Since hard spheres interact only through excluded volume, these packings are in close thermodynamic competition with each other at lower densities. Just above the melting density of monodisperse hard spheres, the fcc crystal is lower in free energy than the

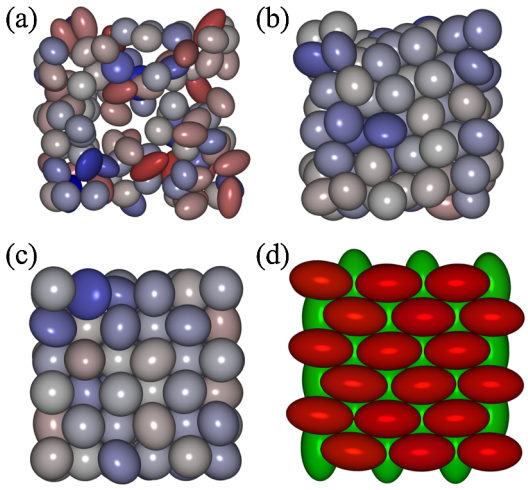

FIG. 3 (color online). Snapshots for stiffness $\beta\kappa = 5$. (a) The fluid phase at low density, (b) the fluid at high density, (c) fcc crystal phase S1 of near-spheres, (d) crystal phase S2 of ellipsoids. Color in (a)–(c) indicates aspect ratio from oblate (blue) to prolate (red). Color in (d) codes for particle orientation.

hcp by a small amount on the order of $10^{-3}\beta^{-1}$ per particle [20]. We have compared the stabilities of the fcc and hcp crystals of deformable spheres near the phase boundary at a few representative stiffnesses κ. For these calculations, the crystals were simulated in a parallelepipedal cell where one angle was approximately $\pi/3$ and the angles and edge lengths were independently adjustable. This allows hexagonal planes to be placed parallel to one of the cell's sides for both crystals, while eliminating any pressure anisotropy. The free energy difference between fcc and hcp stackings was found rapidly to become unmeasurably small for deformable spheres. The S1 solid in Fig. 2 should therefore be regarded as a general hexagonal phase rather than fcc specifically.

Ellipsoids can pack more efficiently than spheres, reaching higher packing fractions both in random [21] and crystalline [22,23] arrangements. The densest known regular packing is $\phi = 0.7707\ldots$ and can be achieved for any ellipsoid of revolution with $x \geq \sqrt{3}$ or $x \leq 1/\sqrt{3}$ [22]. At the least aspherical aspect ratios $x = 3^{\pm 1/2}$ in these ranges, the ellipsoid centers lie on an fcc lattice with the ellipsoid axes parallel in any one face-centered square plane but rotated by 90° from one layer to the next, as depicted in Fig. 3(d). Our deformable spheres can only reach such high packing fractions by adopting this arrangement and so there must be a solid-solid phase transition between the S1 crystal of roughly spherical particles and a second, denser crystal, which we denote S2, where particles are constrained by their neighbors to be permanently ellipsoidal. The existence of this transition was established by preparing the dense crystal and simulating it at high pressure in isobaric MC simulations. As the pressure was gradually decreased, the density suddenly jumped to a lower value and the structure reverted to the S1 crystal of near-spheres.

Given this estimate of the location of the transition, free energy calculations were performed to locate the phase boundary more rigorously. Two additional steps were required in the thermodynamic integration of the dense phase to minimize the interactions between particles at the end point of the integration, close to the reference Einstein crystal. First, the potential for particle deformation was gradually switched from Eq. (1), under which particles strive to become spherical, to (for the prolate case) $U = \kappa(\ln x - \ln\sqrt{3})^2$, so that deformations in the reference crystal are centered on the ideal aspect ratio for the high-density packing. Second, the ellipsoids' orientations were tethered to the idealized directions, alternating for each square plane, using a potential proportional to $\sin^2\theta$, where θ is the angle between the ellipsoid axis and the reference direction [12].

In the limit $1/\beta\kappa \to 0$ of increasing rigidity, the energetic cost of deforming all particles into ellipsoids is so great that the coexistence pressure diverges and the coexisting densities of the two crystal phases are their maximum packing fractions, since all $\phi \leq \pi/\sqrt{18}$ can be

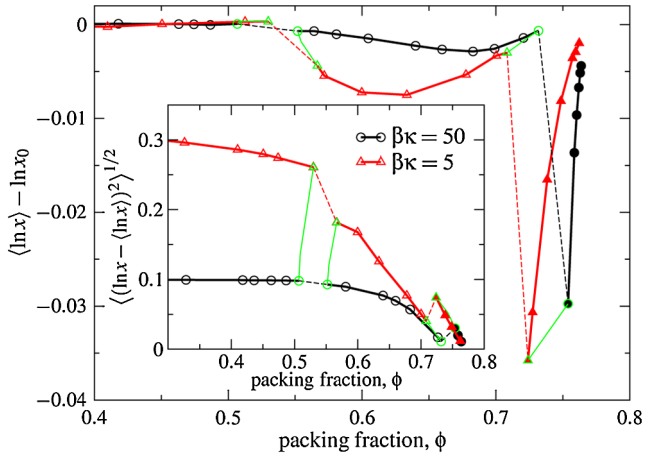

FIG. 4 (color online). Mean ellipsoid aspect ratio x relative to the reference values $x_0 = 1$ (open symbols) in the fluid phase and S1 crystal phase, and to $x_0 = \sqrt{3}$ (solid symbols) in the S2 dense crystal phase for two stiffnesses κ. Inset: standard deviation of the aspect ratio. Dashed lines connect branches of the curves across the phase boundaries. The locus of the phase boundaries is shown by thin green lines.

reached without particle deformation. Since the S2 phase requires $x \neq 1$, the strict hard sphere limit $\beta\kappa = 0$ of the S1-S2 boundary is unattainable and is marked with different symbols in Fig. 2. The effect of increased flexibility is that the reduced energetic cost is balanced by the entropy gain of more efficient packing at progressively lower densities. Hence, the boundaries for the S1-S2 transition move in the opposite direction from those of the fluid-S1 transition in Fig. 2. A spot check at $\beta\kappa = 25$ close to the S2 boundary indicates that the dense phase of ellipsoidal particles is lower in energy than the oblate version by about $0.1\beta^{-1}$ per particle. Both the fluid-S1 and S1-S2 transitions reach a "floppy" limit at $\kappa = 0$, where there is no energetic penalty for deformation. The corresponding packing fractions at coexistence are shown above the top axis of the phase diagram.

Figure 4 shows how the average shape fluctuations of a particle are affected by its local environment. In the fluid phase, particles remain spherical on average, even at high densities, though the range of fluctuations (shown in the inset) narrows with increasing density when κ is small. The transition to the S1 crystal incurs a reduction in the size of the fluctuations compared with the coexisting fluid. In the S1 crystal, there is also a slight preference of particles to be oblate rather than prolate, despite the equal energetic penalty for reciprocal aspect ratios. At the transition to the dense S2 crystal phase, the width of the fluctuation distribution jumps upwards, despite the increase in density. In contrast to the fluid-S1 transition, the concerted deformation and reorganization of the particles generates more space for shape fluctuations.

The introduction and characterization of deformable hard spheres opens the way for studying the effect of flexibility on a variety of colloidal systems. We anticipate that fluid-to-crystal nucleation will be slower for more flexible particles—a factor that may inhibit protein crystallization [7]. Slight asphericity has recently been shown to have a strong effect on crystallizability [24] and the present model permits dynamic, rather than frozen-in, asphericity to be examined. Spontaneous transitions from the fcc phase to the dense crystal of ellipsoids were not observed in our simulations and the transformation pathway is unknown. Finally, the fact that even random packing of nonspherical particles can be more efficient than that of spheres is likely to have a strong influence on jamming and the glass transition [9,25].

The authors are grateful to Dr. Paul van der Schoot, Dr. Eva Noya, and Professor Daan Frenkel for helpful discussions and to EPSRC (U.K.) for financial support.

[1] G. R. Smith and A. D. Bruce, Phys. Rev. E **53**, 6530 (1996).
[2] A. Stradner *et al.*, Phys. Rev. Lett. **99**, 198103 (2007).
[3] A. Lomakin, N. Asherie, and G. B. Benedek, Proc. Natl. Acad. Sci. U.S.A. **96**, 9465 (1999).
[4] A. W. Wilber *et al.*, J. Chem. Phys. **127**, 085106 (2007).
[5] J. Russo, P. Tartaglia, and F. Sciortino, J. Chem. Phys. **131**, 014504 (2009).
[6] P. Eastman, M. Pellegrini, and S. Doniach, J. Chem. Phys. **110**, 10 141 (1999).
[7] P. G. Vekilov and A. A. Chernov, Solid State Phys. **57**, 1 (2003).
[8] G. R. Hendrickson and L. A. Lyon, Angew. Chem., Int. Ed. **49**, 2193 (2010).
[9] J. Mattsson *et al.*, Nature (London) **462**, 83 (2009).
[10] T. G. Mason *et al.*, J. Phys. Condens. Matter **18**, R635 (2006).
[11] B. Farago *et al.*, Phys. Rev. Lett. **65**, 3348 (1990).
[12] D. Frenkel and B. M. Mulder, Mol. Phys. **55**, 1171 (1985).
[13] D. Filip *et al.*, Langmuir **21**, 115 (2005).
[14] D. Frenkel and B. Smit, *Understanding Molecular Simulation* (Academic Press, San Diego, 2002), 2nd ed.
[15] J. W. Perram and M. S. Wertheim, J. Comput. Phys. **58**, 409 (1985).
[16] D. Frenkel and A. J. C. Ladd, J. Chem. Phys. **81**, 3188 (1984).
[17] J. M. Polson, E. Trizac, S. Pronk, and D. Frenkel, J. Chem. Phys. **112**, 5339 (2000).
[18] D. A. Kofke, J. Chem. Phys. **98**, 4149 (1993).
[19] D. A. Kofke and P. G. Bolhuis, Phys. Rev. E **59**, 618 (1999).
[20] A. D. Bruce, N. B. Wilding, and G. J. Ackland, Phys. Rev. Lett. **79**, 3002 (1997).
[21] A. Donev *et al.*, Science **303**, 990 (2004).
[22] A. Donev, F. H. Stillinger, P. M. Chaikin, and S. Torquato, Phys. Rev. Lett. **92**, 255506 (2004).
[23] M. Radu, P. Pfleiderer, and T. Schilling, J. Chem. Phys. **131**, 164513 (2009).
[24] W. L. Miller, B. Bozorgui, and A. Cacciuto, J. Chem. Phys. **132**, 134901 (2010).
[25] L. Berthier and T. A. Witten, Phys. Rev. E **80**, 021502 (2009).